


Microwave diagnostics damage by parametric decay instabilities during electron cyclotron resonance heating in ASDEX Upgrade

S K Hansen^{1,*} , A S Jacobsen² , M Willensdorfer³ , S K Nielsen² , J Stober³ , K Höfler^{4,3} , M Maraschek³ , R Fischer³ , M Dunne³ , the EUROfusion MST1 team⁵ and the ASDEX Upgrade team⁶

¹ Plasma Science and Fusion Center, Massachusetts Institute of Technology, Cambridge, MA 02139, United States of America

² Department of Physics, Technical University of Denmark, DK-2800 Kgs. Lyngby, Denmark

³ Max-Planck-Institut für Plasmaphysik, D-85748 Garching b. München, Germany

⁴ Physik-Department E28, Technische Universität München, D-85748 Garching b. München, Germany

⁵ See Labit B *et al* 2019 *Nucl. Fusion* **59** 086020 for the EUROfusion MST1 team

⁶ See Meyer H *et al* 2019 *Nucl. Fusion* **59** 112014 for the ASDEX Upgrade team

E-mail: soerenkh@psfc.mit.edu

Received 22 March 2021, revised 20 May 2021

Accepted for publication 29 June 2021

Published 20 July 2021



CrossMark

Abstract

We present observations of microwave diagnostics damage in three discharges employing third-harmonic X-mode electron cyclotron resonance heating (ECRH) at the ASDEX Upgrade tokamak. In all cases, the diagnostics damage is explainable in terms of a parametric decay instability (PDI), where an X-mode ECRH wave decays to two trapped upper hybrid (UH) waves near half the ECRH frequency, followed by secondary instabilities, which generate strong microwave signals near multiples of half the ECRH frequency that cause the damage. Trapping of the UH waves near half the ECRH frequency is necessary to reduce the ECRH power required for exciting the PDIs to a level attainable at ASDEX Upgrade, and may occur when the second-harmonic UH resonance of the ECRH waves is present in a region of non-monotonic electron density, e.g. near the O-point of a magnetohydrodynamic mode or the plasma center. The diagnostics damage in the three discharges may be attributed to PDIs occurring near the O-point of a rotating mode, near the plasma center, and near the O-point of a locked mode, respectively. In the rotating mode case, the strong signals are shown to be quasi-periodic, with spikes occurring when the O-point of the mode passes through an ECRH beam, as expected. In the locked mode case, Thomson scattering profiles demonstrate the possibility of the primary

* Author to whom any correspondence should be addressed.



Original Content from this work may be used under the terms of the [Creative Commons Attribution 4.0 licence](https://creativecommons.org/licenses/by/4.0/). Any further distribution of this work must maintain attribution to the author(s) and the title of the work, journal citation and DOI.

PDI occurring based on experimental data for the first time under fusion-relevant conditions. Applying the framework used for ASDEX Upgrade to the X-mode ECRH scenarios planned for the early operation phase of ITER, the PDIs are found to be likely in connection with 170 GHz ECRH of half field scenarios and 104 GHz (or 110 GHz) ECRH of one third field scenarios. Finally, several strategies for mitigating diagnostics damage are proposed.

Keywords: PDI, microwave diagnostics, microwave spikes, wave trapping, ECRH, ASDEX Upgrade, ITER

(Some figures may appear in colour only in the online journal)

1. Introduction

Microwaves are an essential tool in magnetic confinement fusion research due to the strong plasma–wave interactions facilitated by the electron plasma and cyclotron frequencies both being on the order of microwave frequencies in the typical schemes. Well-known uses of microwaves in magnetic confinement fusion research include electron cyclotron resonance heating (ECRH) and current drive [1], as well as electron cyclotron emission (ECE) [2], reflectometry [3–6], and collective Thomson scattering (CTS) [7] diagnostics. Regular models of plasma–microwave interactions for the above applications only consider effects with a linear dependence on the microwave power, as the frequencies and group velocities of the microwaves are usually considered too large to permit significant nonlinear coupling, unless free-electron maser sources are employed [8]. It is, however, well established that plasma–microwave interactions may be significantly modified by nonlinear effects in situations where the effective group velocities of the microwaves, or plasma waves with which they are able to interact, are reduced, as this increases the wave energy densities and reduces the convective losses that normally limit the occurrence of nonlinear phenomena [8]. An example of nonlinear phenomena related to a reduction of the microwave group velocity occurs for X-mode radiation [9] near the upper hybrid resonance (UHR) in conventional tokamak plasmas [10–15]. The present work is, however, focused on nonlinear phenomena associated with reductions of the effective group velocities of the plasma waves interacting with microwave beams, leading to reduced convective losses. We particularly consider the case in which a microwave beam is able to decay into plasma waves trapped around the beam spot, allowing stimulated excitation of the trapped plasma waves at the expense of the microwave beam power [16].

The nonlinear phenomena mentioned above are collectively referred to as parametric decay instabilities (PDIs). PDIs are driven by the free-energy associated with the injected (electromagnetic) pump wave and result in the pump wave decaying to two daughter waves, once the pump wave power exceeds a threshold determined by the interaction strength between the three waves. Additionally, the frequencies of the daughter waves must sum to that of the pump wave to ensure energy conservation. Frequency-shifted daughter waves generated by PDIs lead to strong microwave signals outside the notch filters around the ECRH frequency, which are known to hamper the interpretation of CTS [7, 11–13, 17–21] and

inline ECE [21, 22] measurements. If the daughter waves excited by the primary PDI are trapped, the microwave signals, which are generated by secondary PDIs [19, 23], can become strong enough to damage diagnostics whose receiver views do not overlap with an ECRH beam [18]. In these cases, the PDIs may even lead to conversion of a significant fraction (up to 80% according to current theoretical work [24, 25]) of the pump wave power to daughter wave power, altering the ECRH characteristics from those expected based on linear theories; this point has been demonstrated experimentally in low-temperature plasma filament experiments [26]. Here, we report the first observations of damage to the standard ECE system [2] and a Doppler reflectometer [5], caused by PDIs involving trapped primary daughter waves, during third-harmonic X-mode ECRH at the ASDEX Upgrade tokamak. We further investigate the possibility of such PDIs occurring at the ITER tokamak, along with the microwave diagnostics which may be affected by their occurrence.

Specifically, we consider a primary PDI in which an X-mode pump wave decays to two upper hybrid (UH) daughter waves near half the ECRH frequency. The UH daughter waves near half the ECRH frequency may be trapped around a local maximum of the UH frequency, i.e. around the second-harmonic UHR of the X-mode ECRH radiation when it occurs near a sufficiently sharply peaked local maximum of the electron density along the ECRH beam [15, 18, 19, 23–31]; precise conditions for trapping of the UH waves are discussed in section 2. The above PDIs are thus expected when the second-harmonic UHR occurs near the O-point of a rotating or locked magnetohydrodynamic (MHD) mode [15, 18, 20, 21, 23, 24, 27–31], near the center of low-temperature plasma filaments [26], as well as near the center of magnetically confined fusion plasmas in some cases [18], or near the edge of magnetically confined fusion plasmas in connection with edge-localized modes (ELMs) and blobs [17–19].

As PDIs near the second-harmonic UHR occur in connection with second- and third-harmonic X-mode ECRH, which are the main ECRH schemes of many present-day magnetic confinement fusion devices, they have been the subject of significant experimental [17–22, 26], theoretical [15, 18, 19, 23–31], and numerical [15, 30, 31] investigations since their initial discovery during rotating MHD modes at the TEXTOR tokamak [20, 21]. The original experiments relied on strong microwave signals near the ECRH frequency, observed by the CTS and inline ECE systems, which were subsequently replicated at ASDEX Upgrade [18, 19, 22]. More

recently, signatures of the primary daughter waves near half the ECRH frequency have been observed in low-temperature plasma filaments [26] and at ASDEX Upgrade [18, 19], as well as in numerical simulations [15, 30, 31], confirming the validity of the theoretical framework [15, 18, 19, 23–31]. The microwave signals originally observed near the ECRH frequency originate from combination of the waves near half the ECRH frequency resulting from secondary PDIs [23], which is corroborated by the fact that they require a higher ECRH power than the signals near half the ECRH frequency to occur experimentally [19]. The present paper focuses exclusively on microwave diagnostics damage due to waves near half the ECRH frequency and represents the first study of this kind.

The remainder of this paper is organized as follows. Section 2 describes the theory of trapped-wave PDIs near the second-harmonic UHR, focusing on the plasma and wave parameters for which they may occur. Section 3 presents the damage to the ECE and Doppler reflectometry systems at ASDEX Upgrade during third-harmonic X-mode ECRH, along with the evidence supporting its PDI origin. Section 4 compares the planned experimental conditions in ITER second- and third-harmonic X-mode scenarios to those for which PDIs near the second-harmonic UHR are expected and assesses the potential impact of such PDIs on the microwave diagnostics planned for ITER. Section 5 discusses strategies for mitigating the damage caused by strong microwave signals due to PDIs. Finally, section 6 presents our conclusions.

2. Theory

In a PDI, a strong pump wave decays to two daughter waves once its amplitude exceeds a threshold determined by the non-linear interaction strength between the three waves. Energy and momentum conservation in the three-wave process impose selection rules on the frequencies, f , and wave vectors, \mathbf{k} , of the waves involved in the PDI,

$$f_0 = f_1 + f_2, \quad \mathbf{k}_0 = \mathbf{k}_1 + \mathbf{k}_2, \quad (1)$$

where subscript 0 refers to the pump wave and subscripts 1 and 2 refer to the daughter waves. A PDI involving two trapped daughter waves with similar dispersion relations may occur if the trapped daughter waves have similar frequencies [15, 18, 19, 23–31]; to simplify the analysis, the frequencies of the daughter waves are assumed to be identical in the following, such that $f_1 = f_2 = f_0/2$. The primary PDI occurring near the second-harmonic UHR of an X-mode pump wave particularly involves a pair of UH waves, which have the following dispersion relation for propagation perpendicular to the background magnetic field [18],

$$(k_{j\perp}^\pm)^2 = -\frac{S_j}{2\ell_{Tej}^2} \left(1 \pm \sqrt{1 + \frac{16\pi^2 \ell_{Tej}^2 f_j^2 S_j^2 - D_j^2}{c^2 S_j^2}} \right), \quad (2)$$

where $j \in 1, 2$, $k_{j\perp}^\pm$ is the wave number perpendicular to the magnetic field of the two UH wave branches,

$$\ell_{Tej}^2 = \frac{3f_{pe}^2(T_e/m_e)}{4\pi^2(4f_{ce}^2 - f_j^2)(f_j^2 - f_{ce}^2)}, \quad S_j = \frac{f_j^2 - f_{UH}^2}{f_j^2 - f_{ce}^2},$$

$$D_j = \frac{f_{ce}}{f_j} \frac{f_{pe}^2}{f_j^2 - f_{ce}^2}, \quad (3)$$

with $f_{pe} = \sqrt{e^2 n_e / (4\pi^2 \varepsilon_0 m_e)}$, $f_{ce} = -eB / (2\pi m_e)$, and $f_{UH} = \sqrt{f_{pe}^2 + f_{ce}^2}$ being the electron plasma, electron cyclotron, and (cold) UH frequencies, respectively; e is the elementary charge, m_e is the electron mass, ε_0 is the vacuum permittivity, T_e is the electron temperature in energy units, n_e is the electron number density, and B is the magnetic field strength. The two UH wave branches coincide when $1 + (16\pi^2 \ell_{Tej}^2 f_j^2 / c^2)(S_j^2 - D_j^2) / S_j^2 = 0$, which we shall refer to as the warm UHR; at low T_e , it holds that $|\ell_{Tej} \omega_j / c|^2 \ll 1$, and the UHR condition reduces to $S_j = 0$, which occurs at $f_j = f_{UH}$ and is referred to as the cold UHR. Far from the UHR, the $k_{j\perp}^+$ branch of the UH wave dispersion relation coincides with that of an electrostatic electron Bernstein wave, while the $k_{j\perp}^-$ branch coincides with that of an electromagnetic cold X-mode wave [18]. When a wave from the $k_{j\perp}^-$ branch reaches the UHR, it will be linearly converted to a wave on the $k_{j\perp}^+$ branch, and vice versa [9, 32]. Trapping of a UH wave pair can occur if the two branches propagate on the same side of the warm UHR (since mode conversions are associated with reflections in this case), provided that a region permitting propagation bounded by two UHRs exists along an ECRH beam. Both UH wave branches propagate on the same side of the UHR when $S_j < 0$ and $\ell_{Tej}^2 > 0$, corresponding to $|f_{ce}| < f_j < f_{UH}$ and $|f_{ce}| < f_j < 2|f_{ce}|$, respectively. It is always possible to satisfy the above conditions for some f_j when $f_{UH} < 2|f_{ce}|$, which is equivalent to $f_{pe} < \sqrt{3}|f_{ce}|$, corresponding to underdense and weakly overdense plasmas. Since the plasmas found in conventional tokamaks such as ASDEX Upgrade and ITER are generally underdense, the excitation of trapped UH wave pairs is generally possible when a region with $1 + (16\pi^2 \ell_{Tej}^2 f_j^2 / c^2)(S_j^2 - D_j^2) / S_j^2 > 0$ exists between two UHRs in such systems. In order to illustrate the conditions under which a trapped UH wave pair may exist, we rewrite the propagation condition, using the cold X-mode wave number, k_{Xj} , which satisfies the equation $k_{Xj}^2 = 4\pi^2(f_j^2/c^2)(S_j^2 - D_j^2)/S_j$ [9], yielding $1 + 4\ell_{Tej}^2 k_{Xj}^2 / S_j > 0$, and note that $k_{Xj}^2 > 0$ when the $k_{j\perp}^-$ branch of the UH wave pair is propagating. For $S_j < 0$, $\ell_{Tej}^2 > 0$, and $k_{Xj}^2 > 0$, this is equivalent to

$$\ell_{Tej}^2 < -\frac{S_j}{4k_{Xj}^2}, \quad (4)$$

which may be recast as condition on T_e ,

$$T_e < T_e^c = \frac{(4f_{ce}^2/f_j^2 - 1)(1 - f_{pe}^2/f_j^2 - f_{ce}^2/f_j^2)^2}{12(f_{pe}^2/f_j^2)[f_{ce}^2/f_j^2 - (1 - f_{pe}^2/f_j^2)^2]} m_e c^2, \quad (5)$$

where T_e^c is a critical electron temperature above which propagation of the UH wave pair is no longer possible. For $f_j = f_1 = f_2 = f_0/2$, the $(f_{pe}^2/f_0^2, f_{ce}^2/f_0^2)$ parameter space in which a propagating UH wave pair exists is seen in figure 1.

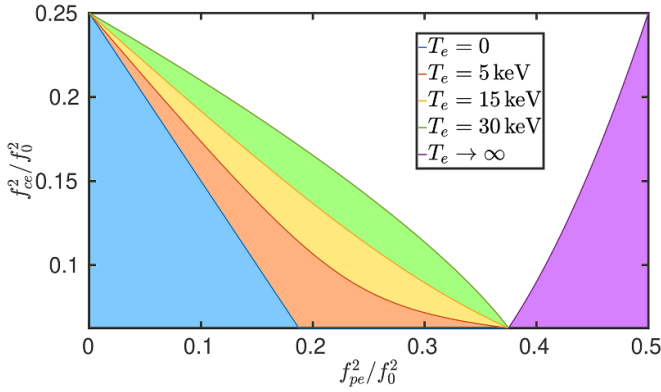


Figure 1. T_e^c versus f_{pe}^2/f_0^2 , f_{ce}^2/f_0^2 , and T_e in the region where $\ell_{Tej}^2 > 0$, when $f_j = f_0/2$; the upper limit of f_{ce}^2/f_0^2 is chosen based on the requirement that $f_j > |f_{ce}|$. No UH wave pair exists in the blue or purple shaded regions at any T_e . For $T_e = 5$ keV, no UH wave pair additionally exists in the orange shaded region, for $T_e = 15$ keV, the yellow shaded region is added to the region with no UH wave pair, and for $T_e = 30$ keV, the green shaded region is finally added.

The points at which $T_e^c \rightarrow 0$ and $|T_e^c| \rightarrow \infty$ represent limits of the space supporting a propagating UH wave pair at all T_e . $T_e^c \rightarrow 0$ when $f_j = 2|f_{ce}|$ and $f_j = f_{UH}$, corresponding to the second-harmonic ECR and the cold UHR of the daughter waves, or the fourth-harmonic ECR and the second-harmonic cold UHR of the pump wave. $|T_e^c| \rightarrow \infty$ when $k_{Xj}^2 \rightarrow 0$, corresponding to the cutoffs of the cold X-mode daughter wave, or the second-harmonic cold X-mode cutoffs of the pump wave; the L-cutoff, characterized by $f_{pe}^2/f_j^2 - |f_{ce}|/f_j = 1$ [9], is of particular interest here. The above lines are depicted in figure 1 and the regions which do not permit propagation of a UH wave pair are shaded in a similar color to the relevant bounding line; the upper limit of f_{ce}^2/f_0^2 in figure 1 is determined by the requirement $f_j > |f_{ce}|$, which is necessary for $S_j > 0$ and $\ell_{Tej}^2 > 0$. We note that the $T_e^c \rightarrow 0$ limit is determined by the requirement that propagating waves from the (electron Bernstein-like) $k_{j\perp}^+$ branch exist, while the $|T_e^c| \rightarrow \infty$ limit is determined by the requirement that propagating waves from the (X-mode-like) $k_{j\perp}^-$ branch exist. At finite T_e , the $T_e^c \rightarrow 0$ limit is displaced toward higher f_{pe}^2/f_0^2 and f_{ce}^2/f_0^2 , as is visible in figure 1. This illustrates the effect of a finite T_e on the location of the second-harmonic UHR, which has important implications for determining whether or not strong microwave signals can be explained in terms of PDIs from this region, as will be shown in section 3. The finite T_e effects on the parameter region allowing propagation of a UH wave pair seen in figure 1 are based on the model of (2) which does not include a relativistic electron response. The validity of (5) is thus restricted to cases where $T_e \ll m_e c^2 = 511$ keV and a more advanced analysis, e.g. considering the relativistic shift of the L-cutoff [33], the harmonics of the ECR and the harmonics of the UHR, as well as the vanishing of the evanescent region for X-mode waves between the R-cutoff and the UHR at high T_e [34], may be of interest. We do, however, note that the displacement of the UHR at finite T_e observed in figure 1 is consistent with the trend found in fully relativistic calculations [34].

Once the existence of a trapped UH wave pair has been established based on n_e , T_e , and B profiles along an ECRH beam, together with the use of (5), the ECRH power threshold which must be exceeded to excite PDIs near the second-harmonic UHR can be calculated by the methods outlined in [18, 19]. More advanced numerical methods, yielding nonlinear saturation amplitudes of the daughter waves, as well as the amplitudes of various microwave signals associated with the PDIs, also exist [23–25, 29], but depend strongly on the precise profiles used and lack a calculation of the stray radiation intensity generated by the PDIs, which is the most likely candidate for diagnostics damage, causing them to fall outside the scope of this paper.

3. Diagnostics damage due to PDIs at ASDEX Upgrade

ASDEX Upgrade is a medium-sized tokamak with a major radius, $R_0 = 1.65$ m, and a minor radius, $a = 0.5$ m [35]. The ASDEX Upgrade ECRH system consists of eight gyrotron sources each delivering up to 1 MW of ECRH power at $f_0 = 140$ GHz in their standard configuration [1, 35]. Additionally, ASDEX Upgrade is equipped with a significant number of plasma diagnostics [35], with the most relevant ones for the present study being the fast ECE [2], Doppler reflectometer [3–5], vertical core Thomson scattering [36], soft x-ray [37, 38], interferometer [39, 40], and locked mode detection [41] systems. Canonical ASDEX Upgrade discharges are heated by X-mode ECRH and operated at a central toroidal magnetic field strength, $B_0 = 2.5$ T, leading to a central second-harmonic ECR [35]. However, operation of X-mode ECRH at a reduced $B_0 = 1.8$ T, which allows the application of resonant magnetic perturbations for ELM suppression [42], is also common and results in a central third-harmonic ECR along with a second-harmonic ECR on the high-field side; the presence of the second-harmonic ECR is useful since the third-harmonic ECR becomes optically thin at low T_e [43], in which case the second-harmonic ECR acts as a beam dump.

To gain an idea about the experimental conditions where trapped-wave PDIs near the second-harmonic UHR are expected in ASDEX Upgrade, we compute n_e at the second-harmonic cold UHR ($f_0 = 2f_{UH}$) of 140 GHz ECRH radiation, n_e^c , assuming a vacuum-like magnetic field $B \approx B_0 R_0/R$, where R is the distance from the symmetry axis,

$$n_e^c = \frac{\pi^2 \epsilon_0 m_e}{e^2} (f_0^2 - 4f_{ce}^2) \approx \frac{\pi^2 \epsilon_0 m_e}{e^2} f_0^2 - \frac{\epsilon_0 R_0^2}{m_e R^2} B_0^2. \quad (6)$$

Plots of n_e^c for $R \in [R_0 - a, R_0 + a]$ with $B_0 = 2.5$ T and 1.8 T, along with the locations of the second- and third-harmonic ECRs, are seen in figure 2. For comparison with an estimate of a lower bound for n_e values in the core of H-mode plasmas [44], figure 2 also shows the line-averaged n_e with the minimum L–H power threshold, \bar{n}_e^{\min} , according to the empirical formula from [45],

$$\bar{n}_e^{\min} [10^{19} \text{ m}^{-3}] = \frac{0.7(I_p [\text{MA}])^{0.34} (B_0 [\text{T}])^{0.62} (R_0 [\text{m}])^{0.4}}{(a [\text{m}])^{1.35}}, \quad (7)$$

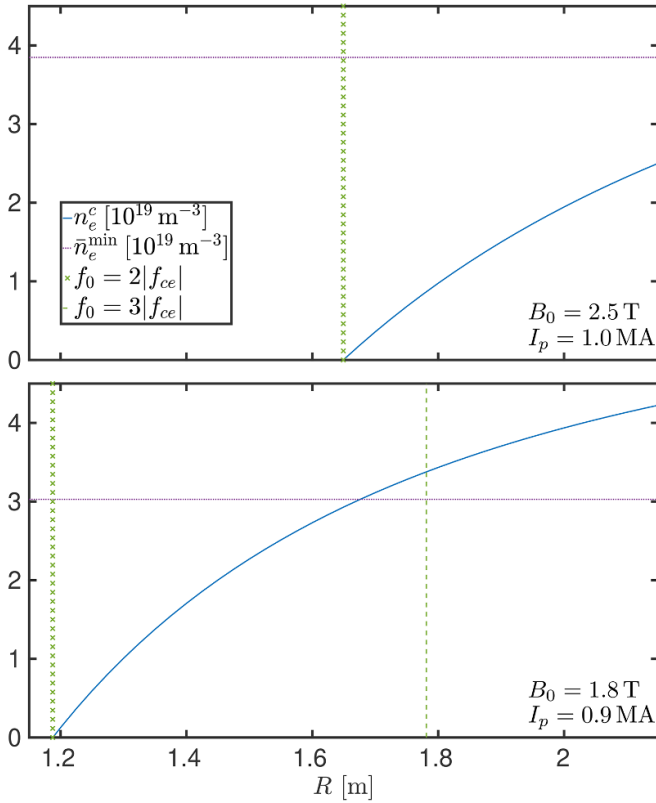


Figure 2. Values of n_e^c (solid lines), as well as the locations of the second- (\times lines) and third-harmonic (dashed line) ECRs of 140 GHz ECRH radiation, versus $R \in [R_0 - a; R_0 + a]$ for a vacuum-like magnetic field ($B = B_0 R_0/R$) and ASDEX Upgrade-like parameters ($R_0 = 1.65$ m, $a = 0.5$ m); \bar{n}_e^{\min} (dotted lines) is also plotted for reference. The upper pane shows the situation for $B_0 = 2.5$ T and $I_p = 1.0$ MA, corresponding to the standard second-harmonic X-mode ECRH scenario at ASDEX Upgrade, while the lower pane shows the situation for $B_0 = 1.8$ T and $I_p = 0.9$ MA, corresponding to the central third-harmonic X-mode ECRH scenario with a second-harmonic ECR beam dump on the high-field side.

at typical values of the plasma current, I_p (1 MA when $B_0 = 2.5$ T and 0.9 MA when $B_0 = 1.8$ T). For $B_0 = 2.5$ T, $n_e^c < 2.5 \times 10^{19} \text{ m}^{-3}$ in the core plasma, which is well below $\bar{n}_e^{\min} = 3.8 \times 10^{19} \text{ m}^{-3}$ at $I_p = 1$ MA. This means that PDIs are only expected in connection with edge phenomena for typical H-mode plasmas, in agreement with previous observations [19]. For $B_0 = 1.8$ T, $n_e^c < 4.25 \times 10^{19} \text{ m}^{-3}$ in the core plasma and exceeds $\bar{n}_e^{\min} = 3.0 \times 10^{19} \text{ m}^{-3}$ at $I_p = 0.9$ MA on the low-field side of the plasma. This makes PDIs near the second-harmonic UHR likely in connection with core MHD activity in H-modes with ELM suppression, as these scenarios require low n_e values in order for the resonant magnetic perturbations to fully suppress ELMs [42]; additionally, the resonant magnetic perturbations further reduce n_e through the electron pump-out effect in these cases [42]. As all the diagnostics damage by PDI-like microwave bursts of interest in the present paper has been observed in $B_0 = 1.8$ T, $I_p = 0.9$ MA, low- n_e H-mode discharges at ASDEX Upgrade, the rest of this section is devoted to describing these scenarios, focusing on

Table 1. Basic parameters of the ASDEX Upgrade discharges considered in this paper.

Case #	1	2	3
ASDEX Upgrade Shot #	35 939	36 149	37 632
I_p (MA)	0.9	0.9	0.9
B_0 (T)	1.8	1.8	1.8
ECE Mixer Degradation (%)	25	40	70
Significant Doppler Reflectometer Damage	No	No	Yes

the observed microwave diagnostics damage and the explanation of this damage based on the trapped-wave PDI theory.

The basic plasma and microwave diagnostics damage parameters in the three discharges of interest, labeled Cases 1–3 for easy reference, are seen in table 1. In all Cases, the strong microwave signals extend up to approximately 80 GHz, which is 10 GHz above half the ECRH frequency; the relatively broad frequency range of the microwave spikes is attributed to the occurrence of secondary PDIs [23, 24]. While frequencies below 73 GHz are not resolved by the microwave diagnostics discussed in this section, (1) and previous observations [19] indicate that strong signals with a similar absolute frequency shift should exist below half the ECRH frequency. Thus, the spikes are considered a threat to microwave diagnostics measuring in the frequency range 60–80 GHz (from $f_0/2 - 10$ GHz to $f_0/2 + 10$ GHz).

Figure 3 shows magnetic plasma equilibria, calculated using the CLISTE code [46], from Cases 1–3. The shown time points are taken from the intervals during which strong microwave signals occur. Additionally, figure 3 shows the cold and warm second-harmonic UHR of the 140 GHz ECRH radiation, obtained by superposing n_e and T_e profiles calculated via integrated data analysis [47] (in Cases 1 and 2) or via vertical core Thomson scattering [36] (in Case 3) on the magnetic equilibria, along with the second- and third-harmonic ECRs, and the central rays of the ECRH beams, computed using a ray tracing code based on the approximations presented in [48, 49]. Finally, for Cases 1 and 3, figure 3 displays the locations and approximate extents of MHD modes identified at the shown time points.

Case 1: PDIs during a rotating (1,1) mode

As illustrated in figure 3, Case 1 has a core MHD mode, identified as a rotating (1,1) mode [44], intersecting the warm second-harmonic UHR slightly on the high-field side of the plasma center. Since this region is also intersected by several ECRH beams, particularly that of the gyrotron located close to the ECE radiometer, the conditions under which PDIs may be excited and generate strong microwave signals at certain phases of the rotating mode are satisfied. Although the ECRH beams pass through the third-harmonic ECR layer before reaching the region where PDIs may be excited, the ray tracing analysis shows that only around 52% of the ECRH power is absorbed before reaching the second-harmonic UHR, owing to the low T_e at the shown time point [43]. This leaves sufficient ECRH power to drive PDIs at the second-harmonic UHR.

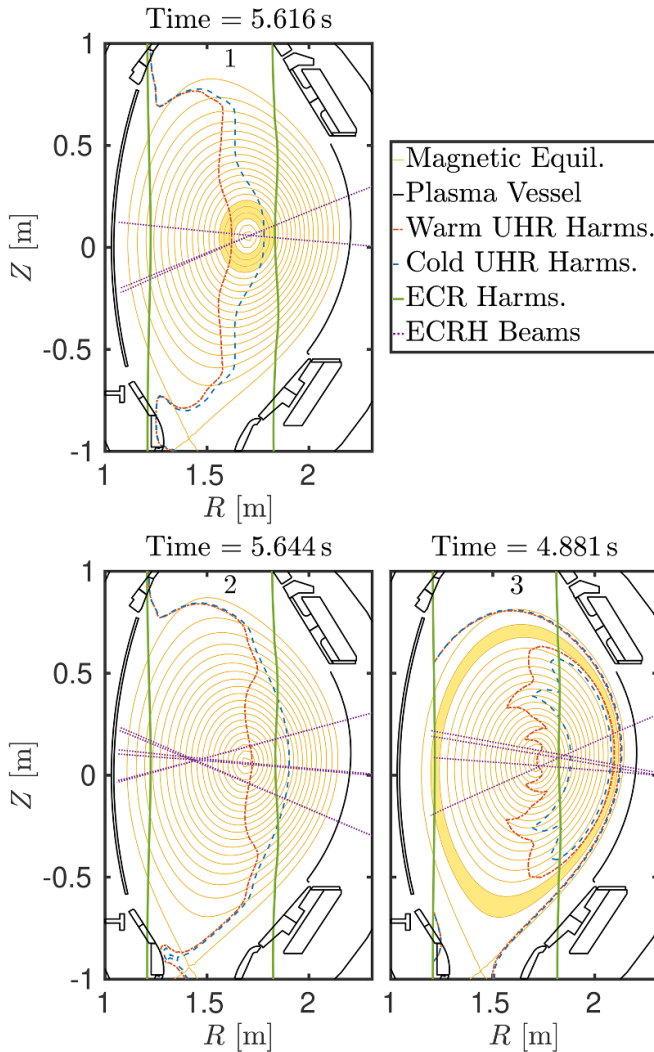


Figure 3. Magnetic equilibria (thin golden lines), calculated using the CLISTE code [46], and the plasma vessel (black lines), along with the second- and third-harmonic ECRs (thick green lines), the cold (dashed blue lines) and warm (dashed-dotted orange lines) second-harmonic UHRs, and central rays (dotted purple lines), calculated using a ray tracing code based on the approximations presented in [48, 49], of the 140 GHz X-mode ECRH beams at ASDEX Upgrade. Panes 1–3 each show a time point from the case of the same number, at which strong PDI-like signals, leading to microwave diagnostic damage, are observed. For Cases 1 and 3, the locations and approximate extents of MHD modes identified at the shown time points are additionally shown by shaded areas.

The above prediction is consistent with the quasi-periodic microwave spikes observed by the fast ECE system [2], which are shown in figure 4.

The fast ECE system is a heterodyne radiometer with 60 channels, a temporal resolution of 1 MHz [2], and is absolutely calibrated using the hot-source method [50]. As the trapped-wave PDIs reach their saturated amplitude on a time scale $\lesssim 1 \mu\text{s}$ in models of typical ECRH experiments [15, 23–25, 28–30], the fast ECE system is generally not capable of characterizing the growth rate of the PDIs; this is discussed for ASDEX Upgrade-specific parameters in connection with Case 3. At $B_0 = 1.8\text{T}$, the ECE system has three

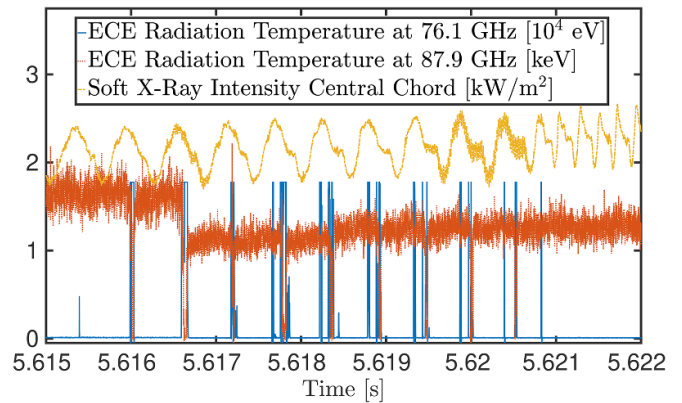


Figure 4. ECE radiation temperatures for the channels at 76.1 GHz (solid line) and 87.9 GHz (dotted line), along with the soft x-ray intensity time trace of a central line-of-sight (dashed line), for time points where strong microwave signals are observed in Case 1. The microwave spikes near half the ECRH frequency (76.1 GHz) occur close to maxima of the soft x-ray intensity, indicating synchronization with the (1,1) mode which is present in the plasma during the shown time interval. After the second large microwave spike, an approximately 25% drop of the ECE radiation temperature observed by the channel at 87.9 GHz is found due to mixer degradation.

down-converter systems (mixers). The damaged system consists of a W-band mixer with a local oscillator frequency of 91 GHz. The lower side band in the frequency region 73–88 GHz is used to measure ECE, whereas the upper side band and frequencies up to 145 GHz, including the 140 GHz ECRH frequency, are rejected by at least 40 dB using a low pass filter. Consequently, this system is not protected against radiation in the frequency region 60–80 GHz. The other two mixer systems in use have filters attenuating the frequency range of 60–80 GHz and were not damaged.

In connection with each microwave spike, the affected mixer of the fast ECE system becomes saturated, which is seen from the fixed maximum ECE radiation temperature measured by the channel at 76.1 GHz during spikes, as well as from the drop in the measured ECE radiation temperature during spikes for the channel at 87.9 GHz, in figure 4. This makes a precise determination of the microwave intensity associated with the PDI-like spikes impossible. Further, and more problematically, the mixer is permanently damaged by the saturation experienced due to the second large microwave spike (at 5.6166 s in figure 4), which may be observed through the approximately 25% drop of the ECE radiation temperature in the channel at 87.9 GHz after this microwave spike. Apart from the fast ECE signal in the channels at 76.1 GHz and 87.9 GHz, figure 4 also includes the soft x-ray ray signal from a channel (H57), which has a line-of-sight passing through the plasma center [37], allowing the phase of the (1,1) mode to be identified. As is evident from figure 4, the microwave spikes close to half the ECRH frequency (at 76.1 GHz) occur for a specific phase of the (1,1) mode, in agreement with what is expected for strong microwave signals originating from PDIs near the second-harmonic UHR.

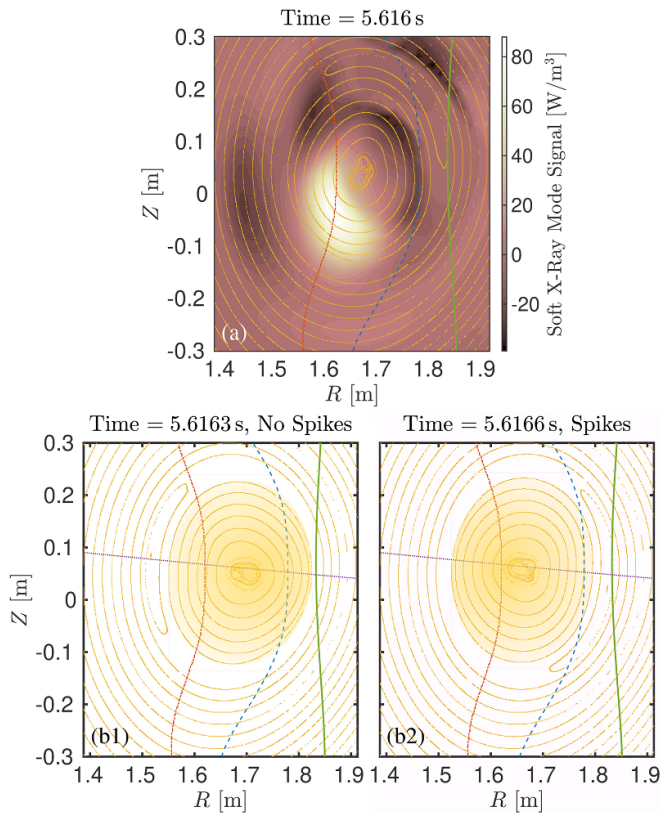


Figure 5. Similar to Case 1 of figure 3 zoomed in on the plasma center, but using a magnetic equilibrium including the (1,1) mode. Pane (a) shows the situation at the toroidal location of the bulk of the soft x-ray pinhole cameras [37] with the tomographic reconstruction of the modification of soft x-ray signal related to the mode [38]; the equilibrium is seen to accurately reproduce the phase of the (1,1) mode. Panes (b1) and (b2) show the situation at the toroidal location of the ECRH beam located near the ECE system at time points without and with microwave spikes, respectively. Strong microwave signals occur when the O-point of the (1,1) mode, marked by the shaded areas in panes (b1) and (b2), passes through the ECRH beam near the warm second-harmonic UHR, cf figure 4.

A more detailed analysis of the structure of the (1,1) mode based on soft x-ray tomography [38] is further carried out. The soft x-ray system at ASDEX Upgrade consists of eight pinhole cameras, all but one of which is located at the same toroidal position [37]. Each pinhole camera contains one to three heads, which include a $75\ \mu\text{m}$ thick beryllium filter and a linear $380\ \mu\text{m}$ thick silicon diode detector array, making the soft x-ray system sensitive to photon energies from approximately 1 keV to 20 keV; the signal from the detectors is sampled at a rate of 2 MHz [37]. The tomography is calculated using data from every available soft x-ray channel and the toroidal location information is included in the calculation. Using the phase information of the (1,1) mode provided by the soft x-ray tomography together with the known spatial structure of a (1,1) mode, it is possible to determine the phase of the (1,1) mode for any toroidal location. As an example, the soft x-ray tomography [38] at the toroidal location of the bulk of the soft x-ray pinhole cameras [37] for the time point of Case 1 in figure 3 is shown with the magnetic equilibrium including the (1,1) mode overlaid in pane (a) of figure 5. While the areas of

increased and decreased soft x-ray signals due to the mode do not exactly match the location of the equilibrium mode structures in the radial direction, the phase of the mode indicated by soft x-ray tomography is accurately captured by the equilibrium including the (1,1) mode. This analysis shows that the PDI-like bursts observed with the ECE system occur when the ECRH beam closest to the ECE system intersects the O-point of the (1,1) mode near the warm second-harmonic UHR, as seen in panes (b1) and (b2) of figure 5. While the correlation of the phase of the (1,1) mode and the microwave spikes is consistent with a PDI origin, as well as previous observations attributed to the same type of PDIs at TEXTOR [20, 21] and ASDEX Upgrade [18], the soft x-ray data alone do not permit a reconstruction of the n_e profile associated with the (1,1) mode, which is necessary for quantitative predictions of the PDI threshold [18], due to their strong dependence on the impurity concentration [37]. This is illustrated by the fact that stronger microwave spikes start occurring in figure 4 without any clear change of the soft x-ray signal associated with the (1,1) mode. We do, however, note that an n_e maximum related to a (1,1) mode, similar to what would be required for UH wave trapping, has been observed by X-mode reflectometry during sawtooth crashes at the Tore Supra tokamak, cf figure 2 in [6]. Further, it is possible to obtain detailed knowledge about the n_e profile associated with a rotating mode by simultaneously firing multiple Thomson scattering lasers [51], but owing to the difficulty of predicting the exact time at which a mode leading to strong microwave signals occurs, as well as the phase of the mode, no such characterization was possible here.

Case 2: PDIs near the plasma center

Case 2 differs from Case 1 in that no strong mode activity is present in the plasma during the time points where the microwave spikes, seen in figure 6, occur. The saturation of the fast ECE mixer is similar to that in Case 1 and after the time interval where strong microwave signals occur, the mixer is again permanently degraded, which can be seen from the approximately 40% drop of the ECE radiation temperature observed by the channel at 87.9 GHz in figure 6. The character of the strong microwave signals is, however, fundamentally different from that in Case 1: rather than quasi-periodic spikes, the signals have a quasi-continuous structure with intermittent quiescent intervals. Such behavior is consistent with microwave signals generated by PDIs in quasi-stationary non-monotonic n_e structures, with the intermittent quiescent phases being caused by n_e fluctuations, which either increase the PDI power threshold beyond the available ECRH power or lead to a transition from a cavity allowing an even-step cascade of PDIs, resulting in a high saturation amplitude of the daughter waves, to an odd-step cascade, resulting in a low saturation amplitude of the daughter waves [24]. Figure 3 indicates that the ECRH beams encounter the warm second-harmonic UHR close to the plasma center, where the n_e profile is generally non-monotonic; while the peaking required for UH wave trapping is not present in the integrated data analysis [47] profile used in figure 3, n_e profiles allowing trapping are within the experimental uncertainties and consistent with

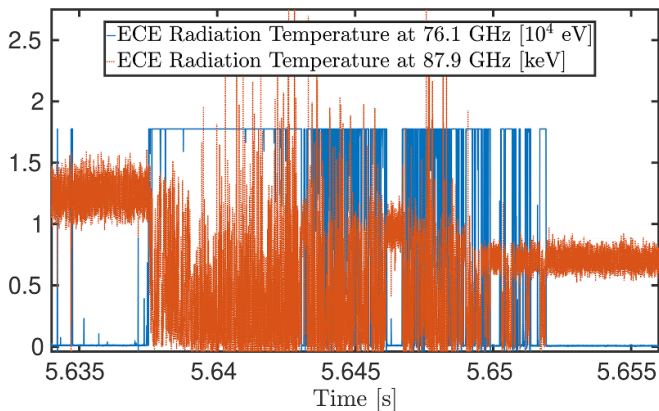


Figure 6. ECE radiation temperatures for the channels at 76.1 GHz (solid line) and 87.9 GHz (dotted line) for time points where microwave spikes are observed in Case 2. The strong microwave signals near half the ECRH frequency have a quasi-continuous structure with intermittent quiescent phases, indicating that they are related to a quasi-stationary structure. After the period during which microwave spikes occur, an approximately 40% drop of the ECE radiation temperature observed by the channel at 87.9 GHz is found due to mixer degradation.

the plasma conditions at the shown time point, as discussed below. Additionally, the gyrotron close to the ECE system is operated at high power (749 kW) during the time interval where strong microwave signals occur, providing a plausible source of the PDI-like microwave spikes observed by the ECE system; although absorption of the ECRH power at the third-harmonic ECR is larger than in Case 1 (around 73% according to the ray tracing analysis), the high-power gyrotron operation means that approximately 200 kW of ECRH power per beam still reaches the plasma center, which is sufficient to drive PDIs near the second-harmonic UHR [19]. We also note that the interpretation of the PDIs occurring near the plasma center hinges on the finite T_e shift of the second-harmonic UHR, as no plausible explanation of the signals in terms of PDIs near the second-harmonic UHR can be found if the cold second-harmonic UHR is used, illustrating the importance of the inclusion of finite T_e effects.

To more firmly establish the possibility of wave trapping near the plasma center, figure 7 shows the n_e profile obtained from integrated data analysis [47] at the time point of Case 2 from figure 3 versus the normalized poloidal flux coordinate, ρ_{pol} ($\rho_{\text{pol}} = 0$ at the plasma center and $\rho_{\text{pol}} = 1$ at the last closed flux surface) [44]. Although the n_e profile obtained from integrated data analysis in figures 3 and 7 does not allow trapping of waves with $f_1 = f_2 = f_0/2$, we note that a slight modification of the n_e profile, also shown in figure 7, is sufficient to allow wave trapping at this time point (as well as from 5.649 to 5.659 s). The errorbars used as limits for the n_e perturbation in figure 7 are the standard deviation of the integrated data analysis n_e profiles during the time interval with strong microwave signals in figure 6 (5.637–5.652 s) and the n_e modification is thus compatible with the experimental uncertainty. Additionally, the central n_e is only monitored by a single line-of-sight of the interferometer system [39, 47]. The interferometer at

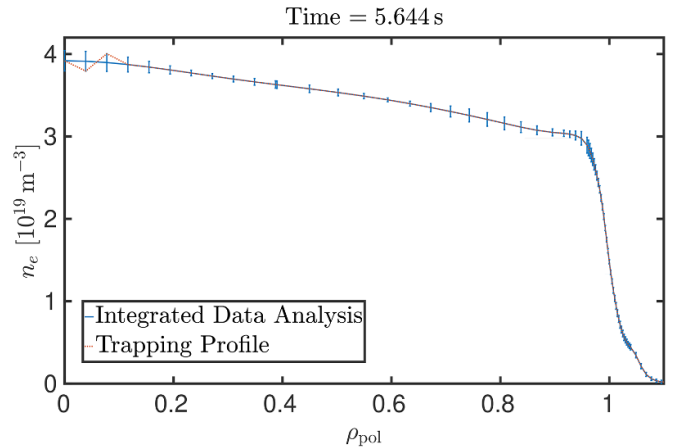


Figure 7. Integrated data analysis n_e profile (solid line) versus ρ_{pol} from Case 2 at 5.644 s (time point shown in figure 3), with errorbars given by the standard deviation of the profiles during the time interval where strong microwave signals are observed in figure 6 (5.637–5.652 s). A profile allowing trapping of 70 GHz UH waves near the plasma center (dotted line) is also shown. The trapping profile is within the errorbars of the integrated data analysis profile and has a similar line-averaged n_e .

ASDEX Upgrade measures the phase shift of a deuterium cyanide laser beam induced by passage through the plasma [39] (at a sampling rate of 1 MHz [40]), which is proportional to the average of n_e along the line-of-sight, a quantity that is left essentially unchanged by the perturbation shown in figure 7.

Finally, the strong microwave signals start occurring ~ 10 ms after a sawtooth crash (at 5.623 s), which is a situation where non-monotonic n_e profiles near the plasma center, resembling the modified one in figure 7, have been observed through X-mode reflectometry at the Tore Supra tokamak, cf figure 2 of [6]. The above discussion illustrates that the n_e profiles of Case 2 are within the experimental uncertainty of ones allowing wave trapping, making the central PDI explanation of the strong microwave signals plausible. However, since the precise central n_e profiles are not measured, no quantitative estimate of the PDI threshold has been made.

Case 3: PDIs during a locked mode

Case 3 is the final discharge in which strong microwave signals leading to mixer degradation have been identified in ASDEX Upgrade so far. Apart from a mixer of the fast ECE system [2], damage also occurred to the mixer of the W-band Doppler reflectometer described by [5], which is sensitive to the frequency range 74–102 GHz, during the microwave spikes in this discharge. The signals observed by the two systems are seen in the upper pane of figure 8 and appear to have a similar character to those observed in Case 2, indicating that they also originate from a quasi-stationary non-monotonic n_e profile along one of the ECRH beams, although we note that the time interval with strong signals is roughly 20 times longer than in Case 2. After the strong microwave signals, an approximately 70% drop of the ECE radiation temperature observed

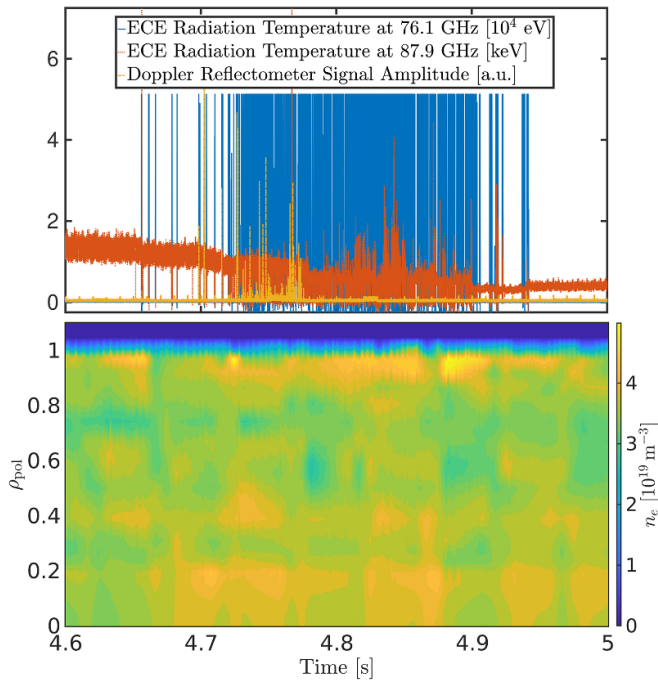


Figure 8. Experimental situation during the time interval in which strong microwave signals are observed for Case 3. The upper pane shows the ECE radiation temperatures for the channels at 76.1 GHz (solid line) and 87.9 GHz (dotted line), along with the signal amplitude of the Doppler reflectometer described in [5] (dashed line). The strong microwave signals near half the ECRH frequency have a quasi-continuous structure with intermittent quiescent phases, indicating that they are related to a quasi-stationary structure. After the period during which microwave spikes occur, an approximately 70% drop of the ECE radiation temperature observed by the channel at 87.9 GHz is found, while the Doppler reflectometer no longer registers any signal, due to mixer degradation. The lower pane shows the n_e profiles obtained from Thomson scattering. During the time points with the strongest microwave signals, a local n_e maximum, related to a locked mode, is visible near the plasma edge ($\rho_{\text{pol}} \in [0.9, 1]$).

by the channel at 87.9 GHz is found, while the Doppler reflectometer no longer registers any signal from the plasma, in both cases due to mixer degradation. From figure 3, it is clear that PDIs occurring near the plasma center provide a possible explanation of the strong microwave signals in this case as well; the ECRH absorption at the third-harmonic ECR is also limited to approximately 49% due to the low T_e in this case, leaving sufficient power to drive trapped-wave PDIs near the second-harmonic UHR. While the gyrotron located closest to the ECE and Doppler reflectometer systems is not active during the period with strong signals, a gyrotron located somewhat further away and pointing toward the sectors containing the ECE and Doppler reflectometer systems is active and may account for the strong microwave signals. This explanation is also consistent with the lack of microwave spikes observed by another Doppler reflectometer [3, 4] located further away from the active gyrotron.

Although a PDI occurring near the plasma center provides a possible explanation of the strong microwave spikes in Case 3, the Thomson scattering and integrated data analysis profiles

themselves do still not permit UH wave trapping near the plasma center. Further, it is unlikely that sawtooth crashes would be able to generate quasi-stationary n_e structures allowing UH wave trapping for ~ 200 ms [6], which would be required to explain the strong signals in the top pane of figure 8, so the physical mechanism allowing UH wave trapping near the plasma center in Case 3 is also unclear. However, another explanation of the strong signals exists in terms of PDIs connected with a locked mode near the plasma edge. As seen from the Thomson scattering n_e profiles in the lower pane of figure 8, along with Case 3 of figure 3, a local maximum of n_e , allowing UH wave trapping, is present near the plasma edge. The lower pane of figure 8 further indicates that the local n_e maximum near the plasma edge ($\rho_{\text{pol}} \in [0.9, 1]$) is present from roughly 4.7 s to 5.0 s. This coincides with the time interval during which a locked mode is present in the plasma and strong microwave spikes are observed, although trapping of UH waves with $f_1 = f_2 = f_0/2$ is only allowed by the profiles for part of the interval. While the toroidal mode number of the locked mode is easily identified as 1, the poloidal mode number is less certain since the mode is essentially locked from its inception, with the only movement being a shift of approximately 77° between 4.6 s and 4.8 s, identified by the locked mode detection system [41]. Analyzing the mode using the framework described in [41], the Thomson scattering laser beam will intersect an O-point near the plasma edge at the time point of Case 3 in figure 3, which is consistent with the observed local n_e maximum, if the poloidal mode number is 4. Additionally, for a poloidal mode number of 4, the ECRH beam suspected of driving PDIs will intersect the mode near an X-point at 4.6 s and closer to, though not exactly at, an O-point at 4.8 s, due to the shift of the mode position; this is consistent with the onset of strong microwave signals after 4.7 s observed in figure 8. Even though the existence of a pure (4,1) mode is somewhat questionable due to its location very close to the separatrix [44], we note that a (4,1) component may be excited through coupling to a (3,1) mode, as previously observed at ASDEX Upgrade [52].

In order to investigate the possibility of PDIs occurring in connection with the locked mode, we compute the PDI power threshold for the ECRH beam suspected of driving PDIs at the time point of Case 3 in figure 3, using the Thomson scattering n_e and T_e profiles, interpolated through piecewise cubic polynomials; the use of a different interpolation method, e.g. spline interpolation, does not yield qualitatively different results. As these profiles do not take the poloidal variation associated with the mode into account and only permit trapping for a limited part of the time interval during which strong microwave signals are observed, this analysis should only be considered indicative. The n_e , T_e , and B profiles extracted along the ECRH beam are seen in figure 9, which also shows the projections of \mathbf{k}_1 and $\mathbf{k}_0 - \mathbf{k}_2$ along the ECRH beam (x direction) for $f_1 = f_2 = f_0/2$, based on (2) and the cold X-mode dispersion relation [9]; upper and lower bounds on the Thomson scattering data mapped to the ECRH beam are further indicated by the errorbars in figure 9. The closed k_{1x}^\pm and $k_0 - k_{2x}^\pm$ curves demonstrate the existence of trapped daughter waves with $f_1 = f_2 = f_0/2$, expected based on figure 3, and the presence of

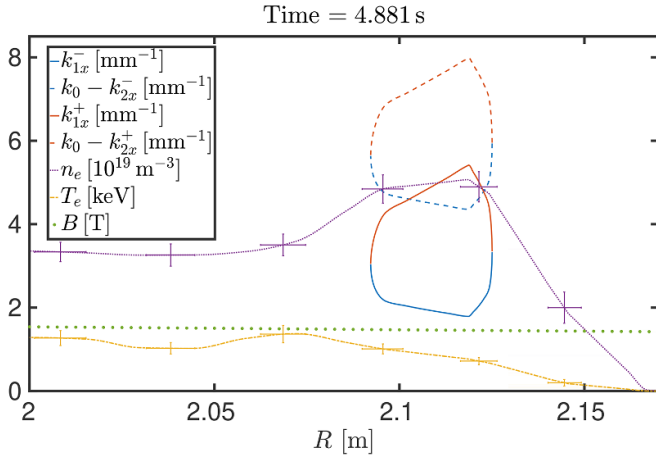


Figure 9. Plasma and wave parameters in the trapping region of the ECRH beam suspected of driving PDIs, with n_e and T_e profiles taken from Thomson scattering, for Case 3 at 4.881 s (cf figure 3). Upper and lower bounds on the underlying Thomson scattering data mapped to the ECRH beam are indicated by the errorbars, while the full n_e and T_e profiles are obtained using piecewise cubic interpolation. At the shown time point, the upper estimate of the PDI power threshold is 72.8 MW, while the lower estimate is 333 kW; the gyrotron power is 889 kW.

points where $k_{1x}^+ = k_0 - k_{2x}^-$ indicates the existence of points satisfying the \mathbf{k} selection rules of (1); both these conditions are necessary for the existence of a low-threshold trapped-wave PDI with $f_1 = f_2 = f_0/2$ [18, 19]. Estimates of the PDI power threshold are provided by the analytical model presented in [18, 19]. An upper estimate of 72.8 MW is provided by assuming convective losses along the poloidal direction to dominate [19], while a lower estimate of 333 kW is provided by assuming diffractive losses along the magnetic field direction to dominate [18]; the experimental gyrotron power of 889 kW is significantly below the upper estimate, but above the lower estimate, necessitating a more detailed discussion of the likelihood that trapped-wave PDIs can be driven by the gyrotron.

If only daughter waves with $f_1 = f_2 = f_0/2$ existed, the upper estimate would be the correct one, and no PDIs would be expected. While good agreement between the experimental PDI threshold and the upper estimate has been found in connection with ELMs at ASDEX Upgrade [19], we note that the UH wave trapping regions in such cases are approximately an order of magnitude shorter than that provided by the locked mode; compare figure 9 with figure 15 of [19]. The increased length of the trapping region significantly increases the number of trapped UH wave modes with frequencies slightly different from $f_0/2$ that may be supported [31] and the assumption of $f_1 = f_2 = f_0/2$ is thus overly simplified. Although the model used here does not permit a detailed study of the different trapped UH wave modes supported by the local n_e maximum, we note that the convective losses along the poloidal direction, which are assumed to dominate in the upper estimate, can be completely suppressed if a pair of UH wave modes are supported in the trapping region without the need for poloidal components of \mathbf{k}_1 and \mathbf{k}_2 to satisfy the Bohr–Sommerfeld

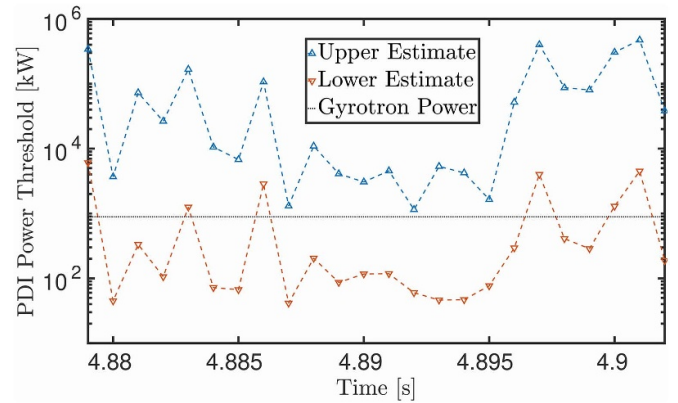


Figure 10. Upper and lower PDI power threshold estimates, along with the gyrotron power, for the ECRH beam suspected of driving PDIs at time points during which the Thomson scattering n_e and T_e profiles, combined with the magnetic equilibria from CLISTE [46], allow trapping of 70 GHz UH waves. The only time point with a Thomson scattering measurement is 4.881 s, so the n_e and T_e profiles at other time points are based on interpolation.

condition [18, 19]. In such cases, diffractive losses along the magnetic field will dominate, and assuming that the nonlinear coupling strength between the daughter and pump waves is not significantly different from the $f_1 = f_2 = f_0/2$ case, the lower estimate will be representative of the actual PDI power threshold. The argument for using the lower estimate is further supported by the fact that theoretical analyses of PDIs near the O-point of MHD modes considering a large number of trapped UH wave modes all find diffraction along the magnetic field to be the dominant loss mechanism [23–25, 29]. Based on the above discussion, we thus conclude that the locked mode near the plasma edge is likely to allow trapped-wave PDIs at the time point of Case 3 in figure 3, meaning that it provides a plausible explanation of the strong microwave spikes at that time point. The growth rate of the instability in figure 9, assuming diffractive losses along the magnetic field direction to dominate, is found to be $6.31 \mu\text{s}^{-1}$, using (4.75) of [18] with the gyrotron power of 889 kW. This growth rate is of a similar order of magnitude to those found in more sophisticated models, which show saturation of the PDIs on a time scale $\lesssim 1 \mu\text{s}$ [15, 23–25, 28–30], further strengthening the claim that the 1 MHz sampling rate of the fast ECE system [2] is insufficient to characterize the growth rate of the PDIs.

As the profiles in figure 9 are obviously based on experimental data possessing a somewhat limited spatial resolution for characterizing the local n_e maximum near the plasma edge, it is interesting to study whether the above conclusion holds for other interpolation schemes and time points as well. The use of different interpolation schemes does not affect the qualitative conclusions significantly, but the upper and lower estimates of the PDI power threshold at different time points are of some interest. Figure 10 shows the PDI power threshold estimates, along with the gyrotron power, for the ECRH beam suspected of driving PDIs at time points around 4.881 s which allow trapping of UH waves with $f_1 = f_2 = f_0/2$. Since 4.881 s is the only time point shown in figure 10 for which Thomson scattering measurements are made, the n_e and T_e profiles of the

surrounding time points are based on interpolation; the magnetic equilibria from CLISTE [46] are, however, updated at each time step. The upper and lower PDI power thresholds observed at 4.881 s are seen to be reasonably representative of the situation throughout the shown time interval: the upper estimate remains above the gyrotron power throughout the period, although it does attain a similar order of magnitude to it at some time points, while the lower estimate remains below the gyrotron power during most of the time points, indicating that PDIs are likely to occur throughout the period in which UH wave trapping is supported by the n_e and T_e profiles.

Although it is not possible to say with certainty whether the strong microwave signals in Case 3 are generated by trapped-wave PDIs near the plasma center, around the O-point of the locked mode, or a combination of the two, it is clear that such instabilities are capable of explaining the occurrence of the microwave spikes.

4. Consequences for ITER

Now that the microwave diagnostics damage at ASDEX Upgrade has been described and shown to be explainable based on PDIs involving trapped daughter waves near the second-harmonic UHR, an application of the above theory to second- and third-harmonic X-mode ECRH scenarios at the ITER tokamak is appropriate in order to assess the relevance and need for mitigation of such phenomena. ITER is a large tokamak, $R_0 = 6.2$ m and $a = 2$ m, with the ultimate goal of demonstrating a fusion power exceeding the auxiliary heating power by a factor of ten [53]. While the high-performance fusion discharges at ITER will be heated using central fundamental O-mode ECRH at $B_0 = 5.3$ T and $f_0 = 170$ GHz, which should not give rise to PDIs near the second-harmonic UHR, a significant number of discharges with X-mode ECRH at one half and one third of the full B_0 ($B_0 = 2.65$ T and $B_0 = 1.8$ T, respectively) are planned for the early operation phase [53]. The scenarios with reduced B_0 allow H-mode access at a lower heating power [45, 54], permitting the pre-nuclear protium or helium-4 plasmas to access H-mode before the full auxiliary heating system is commissioned [53].

At $B_0 = 2.65$ T, the plasmas will have $I_p = 7.5$ MA and be heated by central second-harmonic X-mode ECRH at $f_0 = 170$ GHz, with a possible addition of high-field side fundamental O-mode ECRH at $f_0 = 104$ GHz (or 110 GHz); at $B_0 = 1.8$ T, the plasmas will have $I_p = 5$ MA and be heated by central third-harmonic X-mode ECRH at $f_0 = 170$ GHz, along with central second-harmonic X-mode ECRH at $f_0 = 104$ GHz (or 110 GHz) [53]. To assess the possibility of PDIs near the second-harmonic UHR for the X-mode ECRH scenarios listed above, we plot n_e^c from (6), along with the locations of the second- and third-harmonic ECRs under the assumption of a vacuum-like magnetic field $B \approx B_0 R_0/R$, in figure 11. Additionally, figure 11 shows the Greenwald edge n_e limit, n_e^G , given by the empirical formula [55, 56]

$$n_e^G [10^{20} \text{ m}^{-3}] = \frac{I_p [\text{MA}]}{\pi (a [\text{m}])^2}, \quad (8)$$

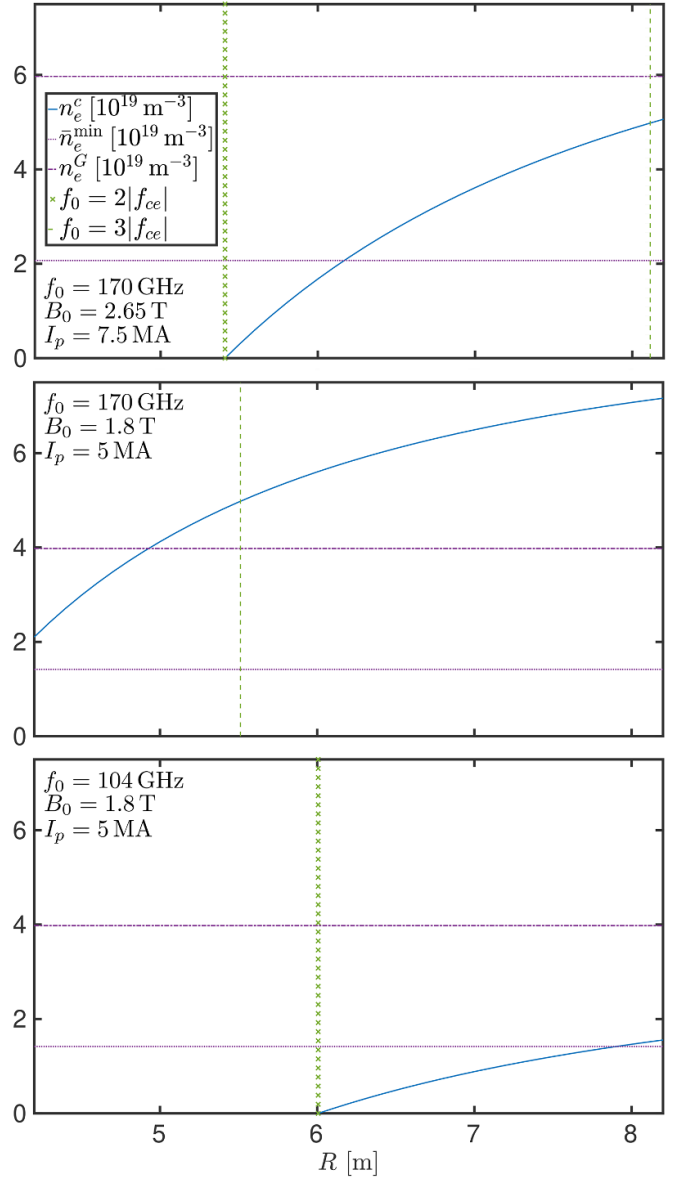


Figure 11. Values of n_e^c (solid lines), as well as the locations of the second- (\times lines) and third-harmonic (dashed lines) ECRs, of ITER X-mode ECRH scenarios versus $R \in [R_0 - a; R_0 + a]$ ($R_0 = 6.2$ m, $a = 2$ m) for a vacuum-like magnetic field ($B = B_0 R_0/R$); \bar{n}_e^{\min} (dotted lines) and n_e^G (dashed-dotted lines) are also plotted for reference. The top pane shows the situation for central second-harmonic ECRH at 170 GHz of the half field ITER scenarios ($B_0 = 2.65$ T, $I_p = 7.5$ MA); the middle pane shows the situation for central third-harmonic ECRH at 170 GHz of the one third field ITER scenarios ($B_0 = 1.8$ T, $I_p = 5$ MA); the bottom pane shows the situation for central second-harmonic ECRH at 104 GHz of the one third field ITER scenarios.

and \bar{n}_e^{\min} from (7) of [45] for the X-mode ECRH scenarios; the \bar{n}_e^{\min} of [53, 54] is $\sim 10\%$ higher, but does not lead to qualitatively different results.

In the half field scenarios with 170 GHz ECRH, n_e^c covers the range from 0 to $0.84 n_e^G$, meaning that the cold second-harmonic UHR will be located in the core plasma, except in cases with n_e close to n_e^G near the plasma edge, which are prone to disruptions [44]. The warm second-harmonic UHR

still occurs for $n_e = 0$ at the second-harmonic ECR but will attain higher values on the low-field side for finite T_e , thus strengthening the above conclusion when warm plasma effects are included. Additionally, the fact that $\bar{n}_e^{\min} = 0.35 n_e^G$ indicates that the half field scenarios of interest will have an edge n_e well below $0.84 n_e^G$, further corroborating the location of the second-harmonic UHR in the core. The half field ITER scenarios are therefore generally expected to be capable of supporting trapped-wave PDIs near the second-harmonic UHR of the 170 GHz ECRH radiation in connection with rotating and locked core MHD modes, generating strong microwave signals around 85 GHz, which would be capable of damaging the ITER low-field side reflectometer [57] and ECE [58] systems, as these will cover the frequency regions of 30–165 GHz and 70–1000 GHz, respectively.

In the one third field scenarios with 170 GHz ECRH, n_e^c covers the range from $0.53 n_e^G$ to $1.80 n_e^G$, although its value at the third-harmonic ECR where most of the ECRH power injected from the low-field side is expected to have been absorbed due to the high central T_e [43], is $1.25 n_e^G$; the inclusion of finite T_e effects will further increase these values for the warm second-harmonic UHR. As the above values are well above n_e^G , and even further above $\bar{n}_e^{\min} = 0.36 n_e^G$, trapped-wave PDIs of 170 GHz ECRH radiation near the second-harmonic UHR are not generally expected to be a problem in one third field ITER scenarios. However, stable operation with core n_e values approaching $2 n_e^G$ has been demonstrated in pellet-fueled discharges at ASDEX Upgrade [56], and if similar experiments were carried out in the one third field ITER scenarios, trapped-wave PDIs near the 170 GHz second-harmonic UHR could be possible in connection with core MHD modes or near the plasma center, which would generate strong signals around 85 GHz, capable of damaging the ITER low-field side reflectometer [57] and ECE [58] systems.

For 104 GHz ECRH in the one third field scenarios, n_e^c covers the range from 0 to $0.39 n_e^G$; the situation is qualitatively similar if 110 GHz ECRH is used instead, as this only leads to a small modification of the upper limit to $0.49 n_e^G$. Since $\bar{n}_e^{\min} = 0.36 n_e^G$ in the one third field scenarios, trapped-wave PDIs near the second-harmonic UHR of 104 GHz (or 110 GHz) ECRH radiation in connection with core MHD modes is a potential issue in such discharges. The PDIs would generate strong microwave signals around 52 GHz (or 55 GHz), which could damage the ITER low-field side reflectometer [57] and CTS [59] systems, as these will cover the frequency regions of 30–165 GHz and 55–65 GHz, respectively.

While no calculation of the precise PDI threshold for the ITER scenarios has been made, due to the arbitrariness of the n_e and T_e profiles that would be used, as well as the uncertainty of the exact ECRH beam widths which will be employed at ITER, we note that the wider ECRH beams expected at ITER compared with ASDEX Upgrade will reduce the PDI power threshold due to diffractive losses, which is found to be the dominant one in current theoretical studies [23–25, 29]. Additionally, the PDI power threshold due to collisional losses will be reduced by the higher T_e and comparable n_e values expected at ITER [53]. There is thus no immediate reason to assume that the PDI power threshold will be significantly higher in ITER

than in ASDEX Upgrade, and since the ITER gyrotrons are expected to have similar power to the ones at ASDEX Upgrade (~ 1 MW per beam) [1, 35, 53], the ECRH beams should generally have sufficient power to drive PDIs in situations where they cross a region allowing trapping of a UH wave pair near $f_0/2$.

5. Mitigation of diagnostics damage

With the ITER scenarios in which trapped-wave PDIs of X-mode ECRH radiation near the second-harmonic UHR may occur and the microwave diagnostics which may be damaged by such PDIs identified, we now discuss strategies for mitigating the damage. The observations from ASDEX Upgrade indicate that the ability of the microwave diagnostics to pick up secondary radiation originating from the ECRH beams plays a key role in determining whether damage will occur or not. This is illustrated by the fact that microwave diagnostics damage has only been observed after the recent upgrade of the ASDEX Upgrade ECRH system [1], which added four gyrotrons distributed throughout the torus to the older system of four gyrotrons, which were located close to each other away from the ECE and Doppler reflectometer systems. In all cases where damage to the ECE and Doppler reflectometer systems was observed, gyrotrons from the new system, with ECRH beams passing close to the diagnostics lines-of-sight, were active, further substantiating the above claim. Additionally, strong enhancement of the PDI-like signals for receiver views overlapping with an ECRH beam in the region where PDIs are expected to occur has recently been demonstrated by the ASDEX Upgrade CTS system in experiments at $B_0 = 2.5$ T [19]. The observations from ASDEX Upgrade also indicate that a frequency region from approximately $f_0/2 - 10$ GHz to approximately $f_0/2 + 10$ GHz may be affected by strong trapped-wave PDI-related microwave signals, presumably due to the occurrence of secondary PDIs involving waves in the lower hybrid and high-order ion Bernstein wave frequency ranges [23, 24].

Thus, although quantitative predictions of the precise frequency and power of the microwave radiation reaching the diagnostics as a result of trapped-wave PDIs are not available as of writing this paper, it is still possible to provide some general guidelines for operating microwave diagnostics in scenarios identified as being prone to the occurrence of trapped-wave PDIs during X-mode ECRH. First, the lines-of-sight of the microwave diagnostics should be oriented away from any ECRH beams to the extent that this is possible, particularly if they have been identified as likely to suffer damage due to trapped-wave PDIs in a given scenario. Additionally, the operation of gyrotrons with ECRH beams passing close to the microwave diagnostics that may be damaged in a given scenario should be minimized. Another mitigation strategy would further be to expand the width of the ECRH beams, since this would reduce the daughter wave saturation amplitudes according to [25]. It is also possible to prevent diagnostics damage by implementing filters blocking radiation from approximately $f_0/2 - 10$ GHz to approximately $f_0/2 + 10$ GHz in front of the

mixers. While the installation of permanent filters blocking such a wide frequency range would severely limit the capabilities of a number of the microwave diagnostics, the installation of variable PIN attenuators, operated with an external bias on a discharge-to-discharge basis or as power limiters [60, 61], could protect the diagnostics in scenarios where damage is likely or on a more permanent basis; the discharge-to-discharge approach has been successful in protecting the ASDEX Upgrade CTS system from PDI-related microwave bursts near the ECRH frequency when viewing an ECRH beam directly [19].

6. Conclusion and outlook

PDI near the second-harmonic UHR have been examined as a source of strong microwave signals capable of damaging microwave diagnostics. The investigations were motivated by observations of microwave spikes near half the ECRH frequency leading to degradation of mixers of the ECE system [2], as well as a W-band Doppler reflectometer [5], in discharges heated by third-harmonic X-mode ECRH at the ASDEX Upgrade tokamak.

Specifically, a primary PDI involving decay of the X-mode pump wave to two UH daughter waves at approximately half the ECRH frequency was investigated. This type of PDI can occur at ECRH powers attainable by the gyrotron sources at ASDEX Upgrade if the UH daughter waves are trapped, since this reduces the convective losses that normally suppress the instability [18, 19, 23–31]. Such trapping may be possible if the electron density profile along an ECRH beam is non-monotonic near the second-harmonic UHR of the ECRH wave, e.g. when the second-harmonic UHR occurs near the O-point of a (rotating or locked) MHD mode or, in some cases, near the plasma center. Once the primary trapped-wave PDI is excited, strong microwave signals capable of escaping the plasma may be generated around multiples of half the ECRH frequency due to the occurrence of secondary PDIs [19, 23, 29], providing a candidate for explaining the diagnostics damage.

Diagnostics damage was observed in three ASDEX Upgrade discharges, labeled Cases 1–3. All discharges were low-density H-modes employing resonant magnetic perturbations, with an on-axis toroidal magnetic field strength of 1.8 T, heated by X-mode ECRH at 140 GHz. This led to a central third-harmonic ECR which was generally optically gray, and a second-harmonic ECR located far on the high-field side, which acted as a beam dump. The relatively low magnetic field strength raised the electron density at which the 140 GHz second-harmonic UHR occurred to levels found in the core plasmas, making the occurrence of trapped-wave PDIs during MHD modes and near the plasma center possible.

In Case 1, a rotating (1,1) mode, coinciding with the second-harmonic UHR, was present in the plasma. The ECE system observed strong microwave spikes in unison with the rotation of the (1,1) mode during a time interval of approximately 5 ms. While a characterization of the electron density perturbations associated with the (1,1) mode was not

possible, a reconstruction of the mode structure using soft x-ray tomography [38] indicated that the microwave spikes were observed when the O-point of the (1,1) mode passed through the ECRH beam located near the ECE system close to the second-harmonic UHR, in agreement with the expectations for microwave signals generated by trapped-wave PDIs. The microwave spikes led to a drop of the ECE radiation temperature observed by the channels operating near half the ECRH frequency of approximately 25% due to mixer degradation.

In Case 2, no rotating mode was present in the plasma, but the second-harmonic UHR was located near the plasma center. This meant that a relatively small perturbation of the central electron density, consistent with the experimental data and seen in figure 7, could explain the strong microwave signals generated during the discharge. Unlike Case 1, the microwave spikes in Case 2 were quasi-continuous, supporting the hypothesis of them being generated in a quasi-stationary structure located near the plasma center. The microwave spikes led to a drop of the ECE radiation temperature observed by channels operating near half the ECRH frequency of approximately 40% due to mixer degradation.

Finally, Case 3 had microwave spikes with a quasi-continuous nature, resembling that of Case 2. Mixer degradation due to the microwave spikes led to a drop of the ECE radiation temperature observed by channels operating near half the ECRH frequency of approximately 70%, and damaged a W-band Doppler reflectometer [5] to the point of it no longer registering any signal from the plasma. While a second-harmonic UHR was present near the plasma center, a more likely explanation of the observed strong microwave signals was provided by the existence of a locked mode near the plasma edge. Analysis of the locked mode using the framework of [41], indicated that a (4,1) mode would be intersected by the Thomson scattering laser beam close to an O-point during the time interval in which strong microwave signals were observed, which would account for the local electron density maximum observed near the plasma edge by the Thomson scattering system. Additionally, the Thomson scattering electron density and temperature profiles allowed trapping of UH waves at half the ECRH frequency for some time points, permitting studies on the possibility of trapped-wave PDIs in the ECRH beams, using the model of [18, 19]. Such investigations showed that trapped-wave PDIs were indeed expected to occur for the relevant ECRH power, provided that trapped UH waves near half the ECRH frequency with negligible poloidal group velocities were supported by the electron density profile.

Thus, the microwave diagnostics damage observed during third-harmonic X-mode ECRH at ASDEX Upgrade was explainable in terms of strong microwave signals generated by trapped-wave PDIs near the second-harmonic UHR in all cases. These results were applied to study the scenarios in which such damage could occur in ITER, based on the research plan described in [53]. Situations allowing the above PDIs were found to be likely for half field discharges (on-axis toroidal magnetic field strength of 2.65 T) heated by 170 GHz second-harmonic X-mode ECRH and one third field discharges (on-axis toroidal magnetic field strength of 1.8 T)

heated by 104 GHz (or 110 GHz) second-harmonic X-mode ECRH. The former PDIs represent a risk to the low-field side reflectometer [57] and ECE [58] systems, while the latter represent a risk to the low-field side reflectometer [57] and CTS [59] systems. Since the above types of discharges will be common during the early operation phase of ITER [53], a number of measures to mitigate potential microwave diagnostics damage have further been suggested. These include minimizing the overlap between ECRH beams and the lines-of-sight of the microwave diagnostics to which they pose a risk, the expansion of ECRH beam widths to lower the PDI saturation amplitudes [25], and the installation of filters blocking frequency regions from 10 GHz above to 10 GHz below half ECRH frequencies in front of the relevant diagnostics, e.g. through variable PIN attenuators operated on a discharge-to-discharge basis or as power limiters [60, 61].

A number of open lines of inquiry concerning trapped-wave PDIs and their consequences for microwave diagnostics at ITER remain. First, it would be useful to analyze UH wave propagation and trapping using a fully relativistic dispersion relation to properly characterize the trapped-wave PDIs under fusion reactor-relevant conditions. Second, theoretical predictions of strong PDI-related microwave signals near 1.5 times the ECRH frequency [29] should be investigated experimentally and their potential consequences for ITER assessed. Third, it would be of interest to carry out investigations similar to the ones found in the present paper for PDIs involving an O-mode pump wave decaying to a single trapped UH wave and a low-frequency daughter wave near the UHR when the UHR occurs near a local maximum of the electron density [62–69]. Such PDIs are predicted to occur in connection with MHD modes for 170 GHz fundamental O-mode ECRH of the full field (on-axis toroidal magnetic field strength of 5.3 T) scenarios and 104 GHz (or 110 GHz) fundamental O-mode ECRH of half field scenarios at ITER [62–64]. Finally, another type of PDIs that may affect 104 GHz (or 110 GHz) fundamental O-mode ECRH in half field scenarios at ITER, discussed in [10–15], could also be investigated.

Data availability statement

The data that support the findings of this study are available upon reasonable request from the authors.

Acknowledgments

SKH acknowledges support by an Internationalisation Fellowship (CF19-0738) from the Carlsberg Foundation. This work was supported by a research Grant (15483) from VILLUM FONDEN. This work has been carried out within the framework of the EUROfusion Consortium and has received funding from the Euratom research and training programme 2014–2018 and 2019–2020 under Grant Agreement No. 633053. The views and opinions expressed herein do not necessarily reflect those of the European Commission.

ORCID iDs

S K Hansen  <https://orcid.org/0000-0002-5146-1056>
 S K Nielsen  <https://orcid.org/0000-0003-4175-3829>
 J Stober  <https://orcid.org/0000-0002-5150-9224>
 K Höfler  <https://orcid.org/0000-0001-7925-8159>
 M Maraschek  <https://orcid.org/0000-0002-3246-7559>
 M Dunne  <https://orcid.org/0000-0002-5259-9970>

References

- [1] Stober J et al 2020 *Plasma Phys. Control. Fusion* **62** 024012
- [2] Hicks N K et al 2009 Upgrades and real time NTM control application of the ECE radiometer on ASDEX Upgrade *Proc. 15th Joint Workshop ECE and ECRH (Yosemite)* ed J Lohr (Singapore: World Scientific) pp 238–44
- [3] Conway G D, Schirmer J, Klänge S, Suttrop W, Holzhauser E and the ASDEX Upgrade Team 2004 *Plasma Phys. Control. Fusion* **46** 951–70
- [4] Conway G D, Angioni C, Ryter F, Sauter P, Vicente J and ASDEX Upgrade Team 2011 *Phys. Rev. Lett.* **106** 065001
- [5] Happel T, Conway G D, Kasperek W, Plaum B, Lechte C, Wagner D, Stroth U and the ASDEX Upgrade Team 2011 Design of a new Doppler reflectometer frontend for the ASDEX Upgrade tokamak *Proc. 10th Intl. Reflectometry Workshop (Padova)* (Padova: Consorzio RFX) pp 1–6
- [6] Nicolas T, Sabot R, Garbet X, Lütjens H, Luciani J F, Guimaraes-Filho Z, Decker J and Merle A 2012 *Phys. Plasmas* **19** 112305
- [7] Nielsen S K, Michelsen P K, Hansen S K, Korsholm S B, Leipold F, Rasmussen J, Salewski M, Schubert M, Stejner M, Stober J, Wagner D and the ASDEX Upgrade team 2017 *Phys. Scr.* **92** 024001
- [8] Porkolab M and Cohen B I 1988 *Nucl. Fusion* **28** 239–54
- [9] Swanson D G 2003 *Plasma Waves* 2nd edn (Bristol: IOP Publishing)
- [10] McDermott F S, Bekefi G, Hackett K E, Levine J S and Porkolab M 1982 *Phys. Fluids* **25** 1488–90
- [11] Hansen S K, Nielsen S K, Salewski M, Stejner M, Stober J and the ASDEX Upgrade team 2017 *Plasma Phys. Control. Fusion* **59** 105006
- [12] Hansen S K, Nielsen S K, Stober J, Rasmussen J, Stejner M and the ASDEX Upgrade team 2019 *EPJ Conf.* **203** 02007
- [13] Hansen S K, Nielsen S K, Stober J, Rasmussen J, Salewski M, Stejner M and ASDEX Upgrade Team 2019 *Phys. Plasmas* **26** 062102
- [14] Senstius M G, Nielsen S K, Vann R G and Hansen S K 2020 *Plasma Phys. Control. Fusion* **62** 025010
- [15] Senstius M G 2020 Simulations of three-wave interactions in microwave heated fusion plasmas *Ph.D. Thesis* Technical University of Denmark Kgs. Lyngby (available at: https://orbit.dtu.dk/files/239590925/MGSenstius_PhD_Thesis.pdf)
- [16] Gusakov E Z and Fedorov V I 1979 *Sov. J. Plasma Phys.* **5** 463–6
- [17] Nielsen S K et al 2016 Three-wave interaction during electron cyclotron resonance heating and current drive *Proc. 41st Int. Conf. Infrared, Millimeter and Terahertz Waves (Copenhagen)* (Piscataway: IEEE) pp 1–2
- [18] Hansen S K 2019 Parametric decay instabilities in the electron cyclotron resonance heating beams at ASDEX Upgrade *Ph.D. Thesis* Technical University of Denmark Kgs. Lyngby (available at: https://pure.mpg.de/rest/items/item_3182239/component/file_3182252/content)
- [19] Hansen S K, Nielsen S K, Stober J, Rasmussen J, Stejner M, Hoelzl M, Jensen T and the ASDEX Upgrade team 2020 *Nucl. Fusion* **60** 106008

- [20] Nielsen S K, Salewski M, Westerhof E, Bongers W, Korsholm S B, Leipold F, Oosterbeek J W, Moseev D, Stejner M and the TEXTOR team 2013 *Plasma Phys. Control. Fusion* **55** 115003
- [21] Westerhof E *et al* 2009 *Phys. Rev. Lett.* **103** 125001
- [22] Bongers W A *et al* 2012 *EPJ Conf.* **32** 03006
- [23] Gusakov E Z and Popov A Y 2016 *Phys. Plasmas* **23** 082503
- [24] Gusakov E Z and Popov A Y 2020 *Plasma Phys. Control. Fusion* **62** 025028
- [25] Gusakov E Z and Popov A Y 2020 *Phys. Plasmas* **27** 082502
- [26] Altukhov A B, Arkhipenko V I, Gurchenko A D, Gusakov E Z, Popov A Y, Simonchik L V and Usachonak M S 2019 *EPL* **126** 15002
- [27] Popov A Y and Gusakov E Z 2015 *Plasma Phys. Control. Fusion* **57** 025022
- [28] Gusakov E Z and Popov A Y 2019 *Nucl. Fusion* **59** 104003
- [29] Gusakov E Z, Popov A Y and Tretinnikov P V 2019 *Nucl. Fusion* **59** 106040
- [30] Sensi M G, Nielsen S K and Vann R G L 2020 *Phys. Plasmas* **27** 062102
- [31] Sensi M G, Nielsen S K and Vann R G L 2021 *Plasma Phys. Control. Fusion* **63** 065018
- [32] Laqua H P 2007 *Plasma Phys. Control. Fusion* **49** R1–42
- [33] Bindslev H 1993 *Plasma Phys. Control. Fusion* **35** 1093–102
- [34] Batchelor D B, Goldfinger R C and Weitzner H 1984 *Phys. Fluids* **27** 2835–46
- [35] Meyer H for the ASDEX Upgrade Team 2019 *Nucl. Fusion* **59** 112014
- [36] Murmann H, Götsch S, Röhr H, Salzmann H and Steuer K H 1992 *Rev. Sci. Instrum.* **63** 4941–3
- [37] Igochine V, Gude A, Maraschek M and ASDEX Upgrade team 2010 Hotlink based soft X-ray diagnostic on ASDEX Upgrade Tech. Rep. IPP 1/338 Max-Planck-Institut für Plasmaphysik Garching (available at: https://pure.mpg.de/rest/items/item_2140623/component/file_2140622/content)
- [38] Odstrčil T, Pütterich T, Odstrčil M, Gude A, Igochine V, Stroth U and ASDEX Upgrade Team 2016 *Rev. Sci. Instrum.* **87** 123505
- [39] Mlynek A, Schramm G, Eixenberger H, Sips G, McCormick K, Zilker M, Behler K, Eheberg J and ASDEX Upgrade Team 2010 *Rev. Sci. Instrum.* **81** 033507
- [40] Mlynek A, Casali L, Ford O, Eixenberger H and ASDEX Upgrade Team 2014 *Rev. Sci. Instrum.* **85** 11D408
- [41] Maraschek M *et al* 2013 *Europhys. Conf. Abstracts* **37D** P4.127 (available at: <http://ocs.ciemat.es/EPS2013PAP/pdf/P4.127.pdf>)
- [42] Leuthold N, Suttrop W, Fischer R, Kappatou A, Kirk A, McDermott R, Mlynek A, Valović M, Willensdorfer M and the ASDEX Upgrade Team and the EUROfusion MST1 Team 2017 *Plasma Phys. Control. Fusion* **59** 055004
- [43] Bornatici M, Cano R, De Barbieri O and Engelmann F 1983 *Nucl. Fusion* **23** 1153–257
- [44] Zohm H 2015 *Magnetohydrodynamic Stability of Tokamaks* (Weinheim: Wiley-VCH)
- [45] Ryter F, Barrera Orte L, Kurzan B, McDermott R M, Tardini G, Viezzer E, Bernert M, Fischer R and the ASDEX Upgrade Team 2014 *Nucl. Fusion* **54** 083003
- [46] McCarthy P J, Martin P and Schneider W 1999 The CLISTE interpretive equilibrium code Tech. Rep. IPP 5/85 Max-Planck-Institut für Plasmaphysik Garching (available at: <http://hdl.handle.net/11858/00-001M-0000-0027-6025-9>)
- [47] Fischer R, Fuchs C J, Kurzan B, Suttrop W, Wolfrum E and the ASDEX Upgrade team 2010 *Fusion Sci. Technol.* **58** 675–84
- [48] Bindslev H 1991 *Plasma Phys. Control. Fusion* **33** 1775–804
- [49] Bindslev H 1992 *Plasma Phys. Control. Fusion* **34** 1601–18
- [50] Hartfuss H J, Geist T and Hirsch M 1997 *Plasma Phys. Control. Fusion* **39** 1693–769
- [51] Kantor M Y, Donné A J H, Jaspers R, van der Meiden H J and TEXTOR Team 2009 *Plasma Phys. Control. Fusion* **51** 055002
- [52] Suttrop W *et al* 1997 *Nucl. Fusion* **37** 119–25
- [53] ITER Organization 2018 ITER research plan within the staged approach (level III – provisional version) Tech. Rep. ITR-18-003 ITER Organization St. Paul-lez-Durance (available at: www.iter.org/technical-reports)
- [54] Martin Y R, Takizuka T and ITPA CDBM H-mode Threshold Database Working Group 2008 *J. Phys.: Conf. Ser.* **123** 012033
- [55] Greenwald M 2002 *Plasma Phys. Control. Fusion* **44** R27–79
- [56] Lang P T *et al* 2020 *Nucl. Fusion* **60** 092003
- [57] Muscatello C M *et al* 2020 *Nucl. Fusion* **60** 066005
- [58] Udintsev V S *et al* 2019 *EPJ Conf.* **203** 03003
- [59] Korsholm S B *et al* 2019 *EPJ Conf.* **203** 03002
- [60] Volkov V V, Ivanova V P, Kuz'michev Y S and Solov'ev Y V 2005 *Tech. Phys. Lett.* **31** 611–12
- [61] Boles T, Brogle J, Hoag D and Curcio D 2011 AlGaAs PIN diode multi-octave, mmW switches *Proc. 2011 IEEE Int. Conf. Microwaves, Communications, Antennas and Electronic Systems (Tel Aviv) (Piscataway: IEEE)* pp 1–5
- [62] Gusakov E Z, Popov A Y, Saveliev A N and Sysoeva E V 2017 *Plasma Phys. Control. Fusion* **59** 075002
- [63] Gusakov E Z and Popov A Y 2018 *Phys. Plasmas* **25** 012101
- [64] Gusakov E Z, Popov A Y and Saveliev A N 2019 *Plasma Phys. Control. Fusion* **61** 025006
- [65] Gusakov E Z and Popov A Y 2021 *Plasma Phys. Control. Fusion* **63** 015016
- [66] Simonchik L, Altukhov A, Arkhipenko V, Gurchenko A, Gusakov E, Popov A and Usachonak M 2019 *Europhys. Conf. Abstracts* **43C** P2.4012 (available at: <http://ocs.ciemat.es/EPS2019PAP/pdf/P2.4012.pdf>)
- [67] Bruschi A *et al* 2017 *Nucl. Fusion* **57** 076004
- [68] Bruschi A *et al* 2019 *EPJ Conf.* **203** 02005
- [69] Baiocchi B, Bin W, Bruschi A, Figini L, Tartari U, Alessi E and D'Arcangelo O 2020 *J. Instrum.* **15** C01046